Applied Surface Science 403 (2017) 717–727

Contents lists available at ScienceDirect

Applied Surface Science

journal homepage: www.elsevier.com/locate/apsusc

Full Length Article

Raman and XPS characterization of vanadium oxide thin films with temperature

Ferran Ureña-Begara[a,*], Aurelian Crunteanu[b], Jean-Pierre Raskin[a]

[a] Université catholique de Louvain, Institute of Information and Communication Technologies, Electronics and Applied Mathematics (ICTEAM), Louvain-la-Neuve, Belgium
[b] XLIM Research Institute, UMR 7252, CNRS/Université de Limoges, Limoges, France

ARTICLE INFO

Article history:
Received 29 November 2016
Received in revised form 14 January 2017
Accepted 16 January 2017
Available online 19 January 2017

Keywords:
Raman spectroscopy
XPS
Vanadium dioxide
Mixed-valence vanadium oxides
Layered oxides
Phase transitions

ABSTRACT

The oxidation mechanisms and the numerous phase transitions undergone by VO_2 thin films deposited on SiO_2/Si and Al_2O_3 substrates when heated from room temperature (R.T.) up to 550 °C in air are investigated by Raman and X-ray photoelectron spectroscopy. The results show that the films undergo several intermediate phase transitions between the initial VO_2 monoclinic phase at R.T. and the final V_2O_5 phase at 550 °C. The information about these intermediate phase transitions is scarce and their identification is important since they are often found during the synthesis of vanadium dioxide films. Significant changes in the film conductivity have also been observed to occur associated to the phase transitions. In this work, current and resistance measurements performed on the surface of the films are implemented in parallel with the Raman measurements to correlate the different phases with the conductivity of the films. A model to explain the oxidation mechanisms and phenomena occurring during the oxidation of the films is proposed. Peak frequencies, full-width half-maxima, binding energies and oxidation states from the Raman and X-ray photoelectron spectroscopy experiments are reported and analyzed for all the phases encountered in VO_2 films prepared on SiO_2/Si and Al_2O_3 substrates.

1. Introduction

The vanadium-oxygen system is very rich due to the numerous valence states of vanadium ranging from V^{2+} to V^{5+}. The stoichiometric oxides of vanadium include VO, V_2O_3, VO_2 and V_2O_5 [1]. Among these oxides, vanadium dioxide (VO_2) and vanadium pentoxide (V_2O_5) have been largely studied. VO_2 is known to exhibit a first order metal-insulator transition (MIT) at $T_c \sim 68$ °C [2]. The MIT is accompanied by a crystal structural change from the monoclinic insulating structure VO_2(M1) below T_c to the tetragonal metallic structure VO_2(R) above T_c [2]. Associated to the MIT, there is a change in resistivity of ~4–5 orders of magnitude [3]. This abrupt change in resistivity makes VO_2 very interesting for electronic and sensing devices [4]. V_2O_5 is the most stable vanadium-oxide composition due to its largest O/V ratio. As a consequence, V_2O_5 is the most common compound resulting from natural aging of vanadium-oxides by oxygen absorption from the atmosphere [5]. V_2O_5 can be described as layers of distorted VO_6 octahedra stacked together and held by weak bond interactions [6,7]. The layered structure and the weak bond interactions suggest that Li^+ ions could be intercalated between the layers to create high-capacity solid-state batteries [8,9]. V_2O_5 is also widely used as a catalyst [10], and very promising in optoelectronics applications due to its electrochromic properties [1]. In addition to these stoichiometric oxides, mixed-valence vanadium oxides with oxidation states between V^{4+}–V^{5+} such as V_6O_{13} and V_3O_7 are also possible. V_3O_7 is a compound with a complex crystal structure formed by layers of VO_5 and VO_6 polyhedra sharing edges and corners [7,11]. V_3O_7 is insulator and stable below 677 °C [7]. V_6O_{13} exhibits metallic character at temperatures above ~−123 °C [7]. The crystal structure of V_6O_{13} is formed by alternated single and double layers of VO_6 octahedra [7]. Due to the layered structure, these mixed-valence oxides are also of great interest for high-energy storage and electrochromic applications [6].

Vanadium oxide thin-films with a specific stoichiometry are often obtained by adequately choosing a lattice-matching substrate and adjusting several parameters including the deposition technique, precursor deposition rate, pressure and temperature [12]. Unfortunately the difficulty of accurately controlling all the parameters and also avoiding the presence of defects results in many cases in undesired stoichiometries and makes the synthesis of these oxides a challenging task [12]. Due to these difficulties,

* Corresponding author.
E-mail address: ferran.urena@uclouvain.be (F. Ureña-Begara).

http://dx.doi.org/10.1016/j.apsusc.2017.01.160
0169-4332/

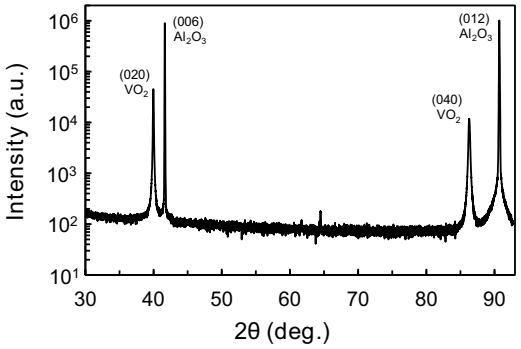

Fig. 1. 0–2θ scan of the 200 nm thick film deposited on Al_2O_3. The small intensity peak at ~65° corresponds to the (009) forbidden peak excited by multiple diffraction.

mixed-valence vanadium oxides are difficult to synthesize and have been less studied. Mixed-valence vanadium oxides however, are commonly encountered in the oxidation/reduction process of VO_2–V_2O_5 [5,13]. The transition mechanisms between the different phases appearing during the process are not well known. Thus, in order to better control the synthesis of vanadium-oxides films with a specific stoichiometry and to understand the mechanisms occurring during the oxidation process of VO_2–V_2O_5, it would be desirable to accurately identify these mixed-valence vanadium oxides.

Raman spectroscopy is a non-destructible technique which allows the characterization of numerous materials with none or minimum sample preparation. The technique has already been used to characterize several stable vanadium oxides including VO_2 and V_2O_5 [5,14–16]. To our knowledge however, there is no comprehensive Raman study of the stoichiometry evolution during the oxidation of VO_2 thin films in air and the experimental data relative to the vibrational modes in mixed-valence vanadium oxides is also very scarce. Relevant information such as full-width half-maxima (FWHM) values are often omitted in the published studies. In addition, there is no proper study comparing the Raman frequencies of VO_2 and V_2O_5 deposited on SiO_2/Si and Al_2O_3. The two substrates are commonly used during the fabrication of vanadium oxides thin films and have very different crystallographic structures. These differences in substrate morphology may affect the characteristics of the vanadium oxide deposited film and as a consequence differences in the Raman signature may appear.

In this work vanadium dioxide thin films deposited on SiO_2/Si and Al_2O_3 are oxidized inside a hermetical thermal stage in ambient air and temperatures in the range R.T.–550 °C. The oxygen absorption when the temperature is increased results in numerous phase changes between the initial VO_2 monoclinic phase and the final and most stable V_2O_5 phase. The different phase changes undergone by the films are investigated by Raman spectroscopy and X-ray photoelectron spectroscopy. Peak frequencies, FHWM, binding energies and oxidation states are reported from the Raman and XPS experiments for all the phases encountered and for the two types of substrates analyzed. Changes in the film conductivity are also observed to occur in parallel with changes in the films stoichiometry. Precise electrical measurements for the current and resistance associated to each phase are reported. Finally, a model to explain the different phase changes observed during the oxidation of the samples is discussed based on the experimental data determined from the Raman and XPS experiments.

The paper is organized as follows. Section 2.1 describes the experimental details for the fabrication of the samples. The Raman

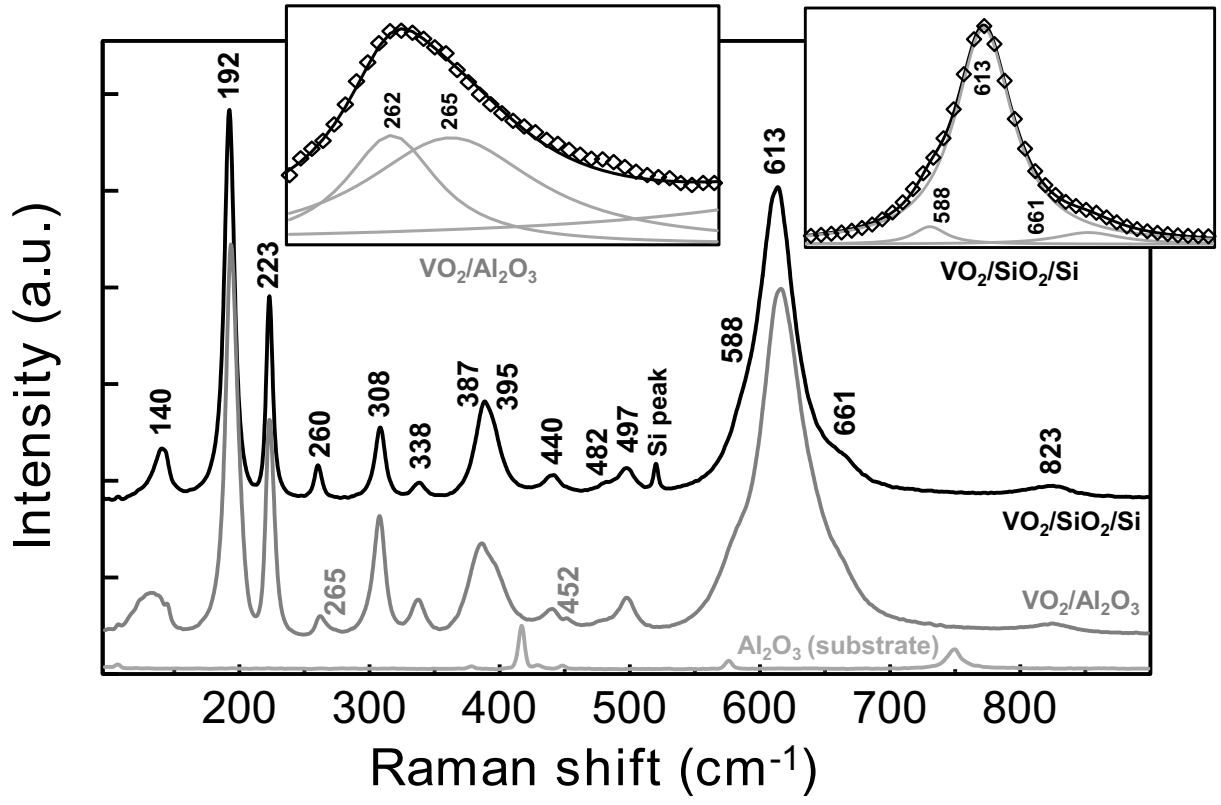

Fig. 2. Raman spectra at R.T. for the VO_2 films deposited on SiO_2/Si and Al_2O_3. For the films deposited on SiO_2/Si, the peak at ~520 cm^{-1} from the silicon substrate is still visible. For the films deposited on Al_2O_3 substrates, the main peak at 417 cm^{-1} is slightly visible (the sapphire spectrum from the films deposited on Al_2O_3 substrates is included as a reference). Insets: Fitting of the 262 and 265 cm^{-1} peaks (left) for the films deposited on Al_2O_3 and the 588, 613 and 661 cm^{-1} peaks (right) for the films deposited on SiO_2/Si.

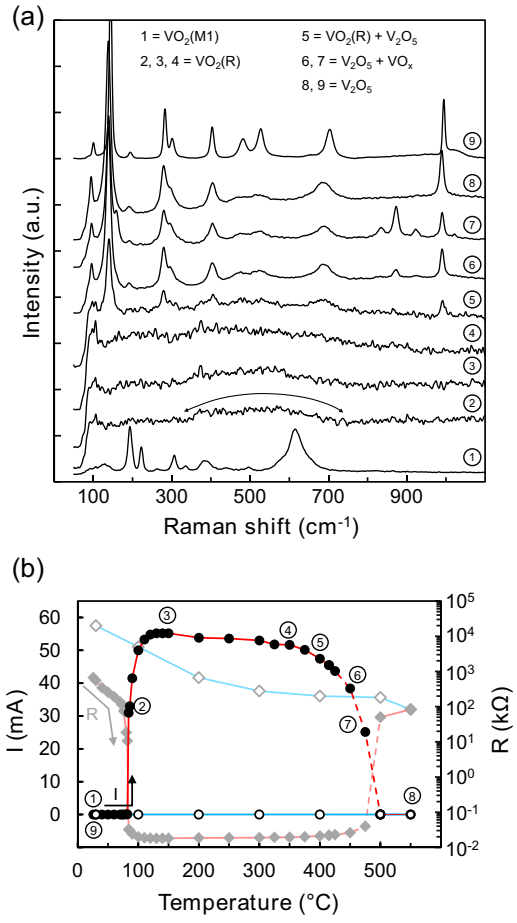

Fig. 3. (Color online) (a) Raman spectrum evolution and (b) current and resistance variation with temperature for the VO_2 films deposited on Al_2O_3. Dotted line indicates the region where the current and resistance evolution is observed to be time (and temperature) dependent.

and XPS setup and the electrical measurements are detailed in Section 2.2. Section 3 presents the results of the Raman and electrical measurements in different temperature ranges (Sections 3.1–3.4). The XPS measurements are presented in Section 4. Section 5 discusses the results and presents a model to explain the different phenomena observed during the oxidation of the samples. Finally, the main conclusions are summarized in Section 6.

2. Experimental details

2.1. Samples fabrication

VO_2 films with thicknesses of 100 and 200 nm were deposited on SiO_2/Si and Al_2O_3 (sapphire) respectively. The films were fabricated by electron beam evaporation of a metallic vanadium target under oxygen atmosphere (P $\sim 8 \times 10^{-2}$ Pa). The films deposited on *c*-type sapphire substrates and on thermally oxidized SiO_2/Si substrates (SiO_2 thickness $\sim$1 mm) were grown at the same conditions at substrates temperatures of $\sim$500 °C and deposition rates of 0.05 nm/s. After the initial deposition step, the films were cooled down at room temperature and submitted afterwards to a post-deposition annealing step at 550 °C under oxygen atmosphere for 15 min (base pressure of 0.5 Pa).

XRD measurements confirmed that the obtained VO_2 films, for both types of substrates, consisted of the monoclinic (M1) phase. The films deposited on sapphire exhibited single (010) orientation with respect to the underlying (001) sapphire substrate (Fig. 1).

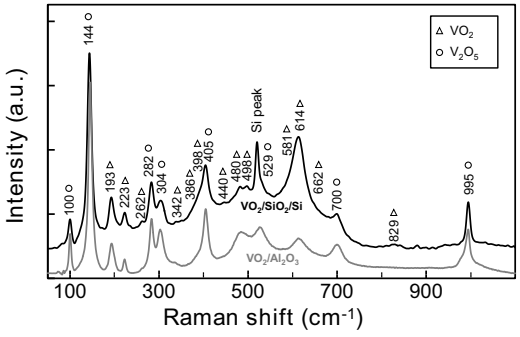

Fig. 4. Raman spectrum of the vanadium oxide films deposited on SiO_2/Si and Al_2O_3 after being oxidized and then cooled down to 30 °C. Films were cooled down immediately after the first peak of the V_2O_5 phase appeared at $\sim$400 °C. A complete mixture between the VO_2 and V_2O_5 phases is observed.

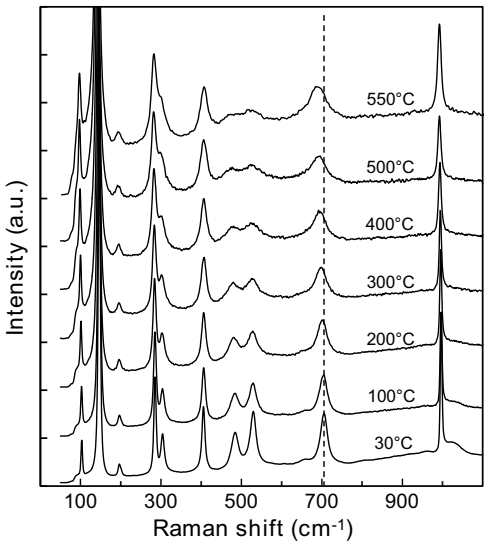

Fig. 5. Raman spectra evolution of the V_2O_5 phase for the films deposited on Al_2O_3 during the cooling process from 550 °C down to 30 °C. A frequency shift with temperature is observed with most of the modes. The largest shift (dotted line) is observed with the mode at $\sim$700 cm^{-1}. A significant increase of the FWHM of this peak with increasing temperature is also observed.

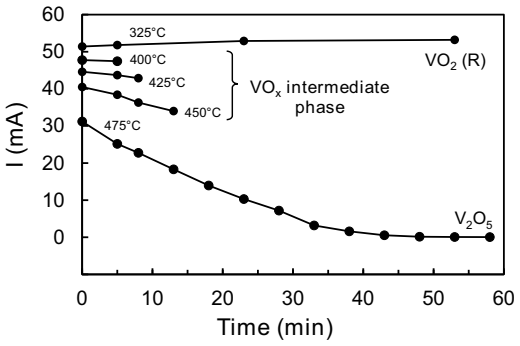

Fig. 6. Current evolution with time and temperature for the 200 nm-thick films deposited on sapphire. Between the MIT temperature and $\sim$325 °C, the film is at the VO_2 rutile phase and the current is constant with time. At temperatures above $\sim$400 °C, the current shows a decrease with time more pronounced with increasing temperature. Raman spectroscopy shows also the formation of a new phase with a vanadium/oxide ratio between 2 and 2.5. At $\sim$475 °C, the current decrease with time is maximized and after $\sim$1 h the film stoichiometry completely changes to V_2O_5.

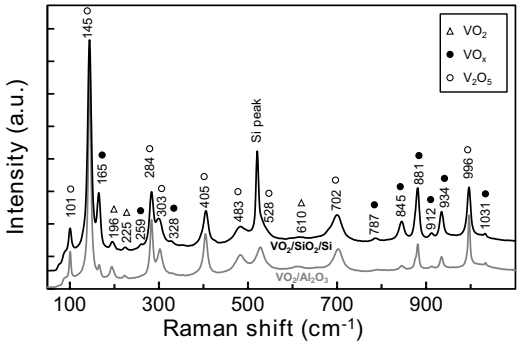

Fig. 7. Raman spectrum of the vanadium oxide films deposited on SiO_2/Si and Al_2O_3 after being oxidized and then cooled down to R.T. Films were cooled down right after the main peaks of the VO_x phase appeared at ~450 °C (black dots).

The films deposited on SiO_2/Si exhibited poly-crystalline orientation (Fig. 9a) with all the peaks assigned to the (M1) phase. Raman analysis in Section 3.1 also confirmed the good quality of the monoclinic phase (M1) on both types of substrates. Additional details about the XRD setup and measurements can be found in Ref. [17].

For the statistical analysis and to favor uniform heating, each film was cut in ~9–12 dies of ~5 x 5 mm^2 each. The dies were heated and characterized individually.

2.2. Raman and XPS setups and measurement conditions

Raman measurements were performed in backscattering configuration using a LabRam HR 800 confocal laser system with a laser wavelength λ = 488 nm and a 2400 gr/mm grating. The spectral resolution for this configuration is ~0.5 cm^{-1}. No polarization was used during the experiments. The laser power delivered to the samples (P_S) was minimized in order to avoid local heating. Avoiding local heating is especially important with vanadium oxide samples since it may cause oxidation or even trigger an undesired phase transition. Local heating usually results in the broadening and redshift of the Raman peaks. Preliminary tests were undertaken for each film to determine the maximum laser power (P_0) that could be delivered to the samples before data interpretation becomes erroneous. After that, an optical density filter was mounted in the laser optical path before reaching the sample to limit the delivered power to 50% of the maximum laser power P_0, i.e., $P_S < 0.5 \cdot P_0$.

The temperature at the sample was controlled by an HFS600E-PB4 thermal stage from Linkam Scientific Instruments. The heating and cooling element of this stage consists of a cylindrical silver block of 22 mm-diameter with a temperature stability ±0.1 °C. The electrical measurements were performed by two tungsten gold plated tips incorporated within the stage and controlled by a Keithley 2400 source meter. A constant voltage of 1 V was applied and the current circulating between the tips was measured as a function of the temperature. The separation distance between the tips was ~1 mm. During the heating and cooling of the sample, a long working distance lens with N.A. = 0.5 was used with the Raman microscope to monitor the film stoichiometry evolution. Measurements at and below 30 °C however, were performed with a X100 magnification lens with N.A. = 0.85 to increase accuracy.

XPS experiments were performed in a ThermoFisher Scientific K-alpha system equipped with a monochromatic AlK_α X-ray radiation (1486.6 eV) in ultrahigh vacuum conditions (base pressure $P \sim 2 \times 10^{-7}$ Pa). Survey scans were performed at constant pass energy (200 eV) and high resolution measurements at 25 eV.

XPS data was analyzed with the CasaXPS software. Mixed Gaussian-Lorentzian functions, *GL(m)*, with *m* representing the Lorentzian percentage, were used to fit the peaks. Several factors affect the optimal mixture percentage including the instrument

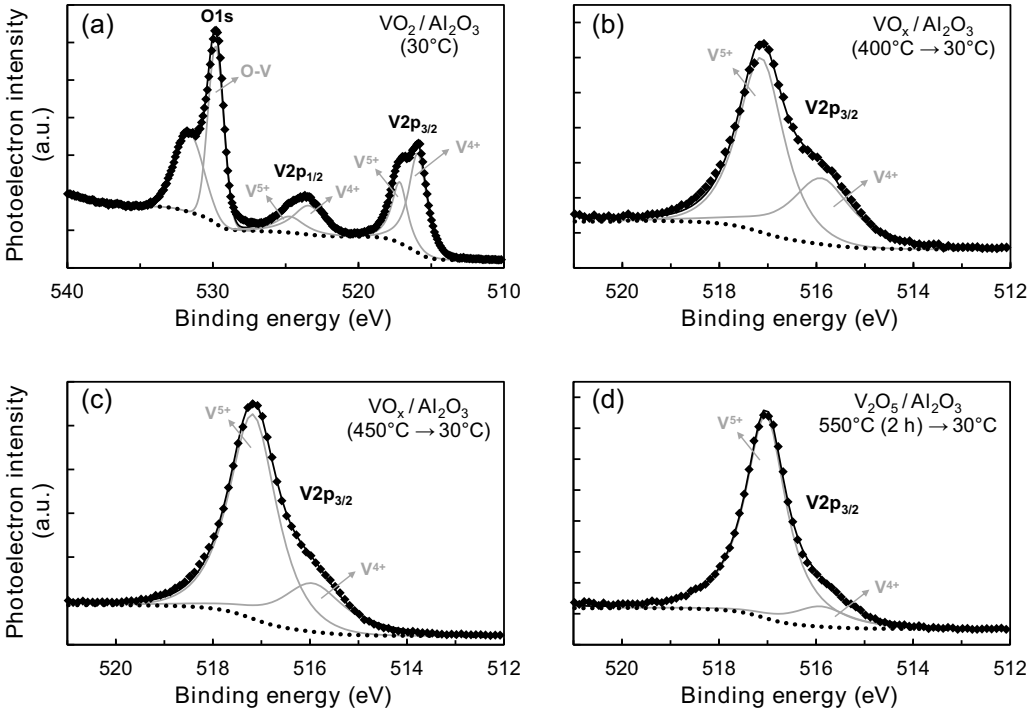

Fig. 8. XPS experimental data, fitted model and peak deconvolution for the vanadium oxide films at different oxidation states. (a) As-received VO_2 films. The O1s energy level is deconvolved into the ~532 eV component, due to surface contamination from C species, and the component at ~530 eV due to O-V bonds. The V2p energy level splits into the $V2p_{1/2}$ and $V2p_{3/2}$ components due to orbital splitting. (b)–(d) $V2p_{3/2}$ peak deconvolution of the films oxidized at 400, 450 and 550 °C, respectively, and subsequently cooled down to 30 °C. Dotted line indicates the Shirley background.

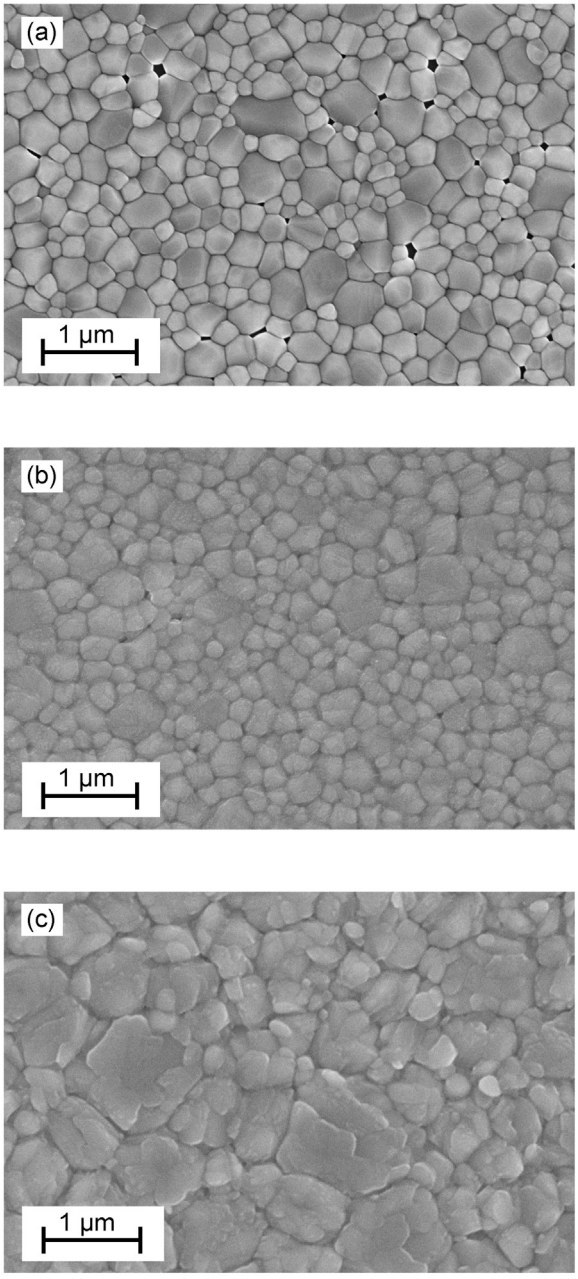

Fig. 9. SEM images of the vanadium oxide films deposited on SiO_2/Si at different oxidation stages at R.T. (a) as-received VO_2, (b) immediately after the appearance at 400 °C of the peaks at ~156, 829, 870 and 921 cm^{-1}, (c) after 2 h oxidation at 550 °C (V_2O_5).

and resolution [18]. In this work, *GL(10–30)* were used to fit the O1s peaks and *GL(70–90)* for the V2p peaks. Values for the binding energies (BE) were charge corrected to the O1s peak at 530 eV. In vanadium oxide compounds, the O1s energy level have shown to be a better reference than the C1s level of adventitious carbon [18]. The area ratio between the $V2p_{3/2}$ and the $V2p_{1/2}$ energy levels, resulting from the orbital splitting of the V2p energy level, was fixed to a 2:1 ratio and the energy separation between the two levels to 7.45 ± 0.10 eV [18,19]. The background between the O1s and V2p peaks was modeled with a Shirley function. The O1s level was included within the Shirley background subtraction since the intensity of this signal is sufficiently strong and the position close enough to the $V2p_{1/2}$ level as to have some influence [19].

Table 1
Raman peak frequencies and FWHM for the as-deposited VO_2 films on SiO_2/Si and Al_2O_3 substrates at R.T.

VO_2(M1)/SiO_2/Si		VO_2(M1)/Al_2O_3	
Freq. (cm^{-1})	FWHM (cm^{-1})	Freq. (cm^{-1})	FWHM (cm^{-1})
140	12.4	–	–
192	8.5	194	9.8
223	4.9	224	6.0
260	4.9	262	6.2
–	–	265	10.8
308	8.5	308	11.2
338	6.5	337	9.5
387	13.3	383	18.4
395	15.8	397	22.4
440	16.2	440	18.4
–	–	452	9.5
482	16.2	477	21.4
497	12.2	498	17.6
588	18.4	580	14.1
613	32.5	616	38.5
661	36.7	656	34.8
823	41.9	823	39.3

3. Raman measurements

3.1. VO_2 films at R.T

Fig. 2 shows the Raman spectra of VO_2 at R.T. for the films deposited on SiO_2/Si and Al_2O_3. The peak in the Raman spectrum at ~520 cm^{-1} of the 100 nm-thick films deposited on SiO_2/Si relates to the first order Si peak from the Si substrate. For the 200 nm thick-films deposited on Al_2O_3, the main peak of the sapphire substrate at ~417 cm^{-1} is still slightly visible. This indicates that the penetration depth for the 488 nm radiation on VO_2(M1) is ~200 nm and that the radiation has probed the entire film thickness.

Above the MIT temperature, if no external strain is applied, VO_2 exhibits a tetragonal phase (rutile) with $P4_2/mnm$ symmetry. In this phase, each vanadium atom is at the center of an oxygen octahedron aligned along the *c*-axis direction. Oxygen octahedra share edges with neighboring octahedra along the *c*-axis and corners with neighboring octahedra in the (001) plane [20]. Below the MIT temperature, VO_2, with no applied external strain, crystallizes in the monoclinic M1 phase with $P2_1/c$ symmetry [20]. In this phase, the vanadium atoms dimerize and tilt with respect to the rutile *c*-axis [20]. The $P2_1/c$ space group has 18 Raman active modes with A_g and B_g symmetries [15]. Most of these modes are visible at R.T. with no applied polarization (Fig. 2). For clarity, only the peak frequencies corresponding to the films deposited on SiO_2/Si are shown in Fig. 2. Table 1 details the average peak frequencies and full-width half-maxima obtained for all the films on both substrates (SiO_2/Si and Al_2O_3). The lowest frequency peak at ~140 cm^{-1} has been ascribed to soft phonon vibrations [15,21]. The existence of a soft-phonon (associated with the electron-phonon mechanism during the phase transformation in VO_2), has however long been debated [22–24]. For the films deposited on Al_2O_3, a broader and redshifted peak, compared with that of the films deposited on SiO_2/Si, is observed. As shown in Fig. 2, the Raman signature of Al_2O_3 from the substrate (included as a reference in Fig. 2) shows no peak nearby the ~140 cm^{-1} frequency. This suggests that the broadening of the peak may result from additional modes appearing at the interface between the VO_2 layer and the Al_2O_3 substrate. Low frequency modes nearby the ~140 cm^{-1} frequency have already been reported in many layered vanadium oxides [5]. The low frequency modes arise as a result of the relative motions between the units constituting the layered structure [5]. In case of the films deposited on Al_2O_3, layered modes may result from the interface between VO_2 and Al_2O_3 due to the similar lattice spacing between the two materials. A

non-homogenous layered structure would result in multiple low frequency modes adding together and broadening the ~140 cm^{-1} peak.

The peaks at ~192, 223, 260, 308, 338, 387, 395, 440, 482, 497, 588, 613, 661 and 823 cm^{-1} are readily assigned to the VO_2(M1) phase [14,15,22], (the broad peak at ~613 cm^{-1} is a convolution of the peaks at 588, 613 and 661 cm^{-1} (Fig. 2, right inset)). The low frequency phonons at 192 and 223 cm^{-1} relate to lattice motion involving V—V bonds [20]. The rest of the peaks are assigned to vibrational modes of V—O bonds [20]. In addition to these peaks, another mode at ~265 cm^{-1} has been reported [15]. Due to the low intensity and the proximity to the 260 cm^{-1} peak, the characterization of the 265 cm^{-1} mode at R.T. has always been challenging [15,25]. In order to accurately characterize the peak at ~265 cm^{-1}, the acquisition time for the films deposited on Al_2O_3 was increased up to ~1 h (Fig. 2, left inset). For the films deposited on SiO_2 however, the peak at ~265 cm^{-1} was not observed despite the increase in the acquisition time. Several factors, including temperature and strain are known to affect the peak position, the full-width at half-maximum (FWHM), and the intensity of the Raman peaks [26]. Internal strain in VO_2 films originates as a result of the differences in thermal expansion coefficients between the VO_2 film and the underlying substrates during the high temperature deposition process and the subsequent cooling [17]. Due to a larger difference in thermal expansion coefficients between VO_2 and SiO_2 ($\alpha_{VO2}/\alpha_{SiO2}$ ~40) [27,28], compared with that between VO_2 and Al_2O_3 ($\alpha_{VO2}/\alpha_{Al2O3}$ ~4) [27,28], the films deposited on sapphire will undergo less internal strain than those deposited on SiO_2. This difference in internal strain explains also some of the discrepancies observed in Table 1 between the frequencies observed with the two types of substrate. As shown in Table 1, the larger discrepancies are observed with the high frequency peaks at ~588, 613 and 661 cm^{-1}. The frequencies of these peaks mainly involve oxygen bonds connecting vanadium chains along the *c*-axis [20]. These frequencies scale with the reduced masses of the oxygen and vanadium atoms and are expected to be highly affected by strain. Other factors including the spectral resolution of the equipment and the uncertainties introduced during the peak deconvolution may also affect.

3.2. VO_2 films at temperatures in the range 30–350 °C

In order to monitor the changes in the film structure with temperature, Raman spectra were acquired at different temperatures in the range 30–550 °C during the heating and the cooling cycle. The current and resistance variation of the film with temperature was monitored in parallel with the Raman measurements during the complete temperature cycle. Fig. 3 shows the Raman spectrum evolution and the I(T) and R(T) variations for the films deposited on Al_2O_3.

Upon heating the films above the MIT temperature (~68–75 °C), the initial monoclinic phase changes to rutile. The Raman spectrum of the rutile phase (curve 2 in Fig. 3a) is dominated by a prominent luminescence background, indicative of the metallic behavior of the rutile phase, and a broad peak which extends from ~300 to 750 cm^{-1} (arrow in Fig. 3a) [29,30]. The change from the monoclinic structure to rutile is also accompanied by a large change in resistance, ~3–4 orders of magnitude (point 2 in Fig. 3b). This phase transition is reversible with temperature, i.e., a temperature decrease down to R.T. results in the monoclinic phase (M1) being recovered. The temperature onset for the recovery of the monoclinic phase is however lower during the cooling cycle than during the heating cycle. This difference results in a thermal hysteresis whose width has been related to the film grain morphology [31].

As observed in Fig. 3b, the current (resistance) reaches its maximum (minimum) value at ~150 °C (point 3 in Fig. 3b). The film, as evidenced by the Raman spectrum, remains at the rutile phase up to ~350 °C (point 4 in Fig. 3a). During this temperature range, ~150–350 °C, the current (resistance) slowly decreases (increases) at ~–20 μA/°C. This slow decrease (increase) in current (resistance), is ascribed to an increase in carrier scattering with increasing temperature characteristic of the metallic behavior of the rutile phase.

3.3. VO_2 films at temperatures in the range 350–400 °C

Between ~350–400 °C, the characteristic Raman spectrum of the rutile phase starts changing. A new peak at ~136 cm^{-1} emerges at ~375 °C followed by other peaks with lower intensity at ~400 °C (curve 5, Fig. 3). This change in the Raman spectrum indicates that a change in stoichiometry is taking place at the surface of the film (oxidation). In parallel with the appearing of these new peaks, an increase in the current (resistance) variation with temperature is observed (~-80 μA/°C) compared with that measured during the previous temperature range ~150–350 °C (~-20 μA/°C).

In order to identify the new peaks, two additional experiments were performed. In a first experiment, the temperature was decreased down to 30 °C immediately after the appearance of the 136 cm^{-1} peak. During the cooling process, N_2 was pumped into the chamber to minimize the oxidation. The output valve of the thermal chamber was kept open during the pumping process to allow N_2 to flow and replace air within the chamber. The Raman spectra of the two films at 30 °C (Fig. 4) reveal that the VO_2(M1) phase is still present (triangles in Fig. 4) although some other peaks not related to the VO_2(M1) phase are also observed. By comparison with the literature these other peaks can be ascribed to the V_2O_5 phase (open circles in Fig. 4) [5,32,33]. The peak frequencies of the V_2O_5 phase at 30 °C were however shifted compared with the frequencies observed at 400 °C. To confirm that the peaks observed at 400 °C relate to the V_2O_5 phase and the observed shift is only due to a temperature gradient, a second experiment was performed with a new set of samples. This is important since some vanadium oxides such as V_6O_{13} have a crystal structure very similar to that of V_2O_5 and exhibit also a similar Raman spectra [5]. In this second experiment, the samples were heated up to 550 °C and maintained at this temperature for 2 h for a complete oxidation. After that, the samples were progressively cooled down to 30 °C. Fig. 5 shows the evolution of the Raman spectra for the samples deposited on Al_2O_3 during all the cooling process from 550 °C down to 30 °C. No sign of the VO_2 phase was observed in this second experiment and all the frequency peaks measured at 30 °C perfectly agreed with those previously reported for the V_2O_5 phase [5,32,33], indicating that the samples had completely oxidized. The shape and peak positions of the spectra at 400 °C (Fig. 5) coincided with the peaks ascribed to the V_2O_5 phase in the first experiment also at 400 °C. This confirmed that the phase observed during the first experiment at 400 °C was the V_2O_5 phase. Table 2 summarizes all the peak positions and FWHM determined for the V_2O_5 phase at 30 °C. As observed in Fig. 4 however, the V_2O_5 phase appears mixed with the VO_2(M1) phase. This denotes that not all the VO_2 in the bulk of the films has converted to V_2O_5. The VO_2 observed at 400 °C is however in the rutile phase as evidenced by the luminescence background and the still visible broad peak extending from ~300 to 750 cm^{-1} characteristic of the VO_2(R) phase (curve 5, Fig. 3). This is in contrast to the monoclinic phase of VO_2 observed at 30 °C in Fig. 4.

V_2O_5 belongs to the orthorhombic space group with P_{mnm} symmetry. From symmetry considerations and under the factor group D_{2h}, 21 vibrational modes are expected to be Raman active [34]. With the Raman setup detailed in Section 2.2, the Raman modes observed in this work were found at ~102, 145, 197, 284, 304, 405, 481, 528, 700 and 995 cm^{-1} (only minor differences in the frequencies of the Raman modes between the two substrates were found) (Table 2). The lowest frequency modes at ~102, 145 and 197

Table 2
Raman frequencies and FWHM at R.T. for the films obtained after 2 h being oxidized at 550 °C (V_2O_5 phase) on SiO_2/Si and Al_2O_3 substrates.

$V_2O_5/SiO_2/Si$		V_2O_5/Al_2O_3	
Freq. (cm^{-1})	FWHM (cm^{-1})	Freq. (cm^{-1})	FWHM (cm^{-1})
102	4.6	102	4.1
145	6.5	145	5.6
197	6.2	197	7.4
284	7.3	284	6.5
304	12.6	304	10.4
405	10.3	405	8.6
481	26.9	483	21.9
528	22.0	528	20.5
700	24.2	702	21.3
995	5.7	995	4.6

Table 3
Raman peak frequencies and FWHM for the films obtained at ~450 °C and subsequently cooled down to 30 °C on SiO_2/Si and Al_2O_3 substrates. The data correspond to a vanadium oxidation state ~4.6–4.7. Peaks corresponding to the V_2O_5 phase are not included for clarity.

$VO_x/SiO_2/Si$		VO_x/Al_2O_3	
Freq. (cm^{-1})	FWHM (cm^{-1})	Freq. (cm^{-1})	FWHM (cm^{-1})
165	5.8	167	3.4
787	21.4	791	34.4
845	15.7	845	17.6
881	8.3	881	7.9
912	10.8	912	19.5
934	11.0	934	9.8
1031	10.2	1033	7.5

cm^{-1} can be ascribed to layered modes (external modes) in V_2O_5 [16]. The intermediate frequency peaks at ~284, 304, 405, 481, 528 and 700 cm^{-1} relate to the bending and stretching vibrations (internal modes) of vanadium-oxide bonds in V_2O_5. The highest frequency peak at ~995 cm^{-1} corresponds to the stretching mode of the terminal oxygen (vanadyl). The vanadyl bond is the shortest vanadium-oxygen bond in V_2O_5. The peak position of the vanadyl bond at ~995 cm^{-1} agrees with that reported for bulk crystal (~994 cm^{-1}) [34]. The agreement in the vanadyl peak position with that reported for bulk and the absence of a mode at ~840 cm^{-1}, reported to become Raman active in defective V_2O_5, confirms the good crystallinity of the V_2O_5 phase within the film [16].

As a final remark from this experiment, it was observed that once the 136 cm^{-1} peak appears (indicative of the formation of the V_2O_5 phase), the structural changes in the films are not reversible when the temperature is decreased down to R.T., i.e., the initial VO_2(M1) phase and the V_2O_5 phase coexist in a proportion which depends on the degree of oxidation undergone. This is in contrast to the complete reversibility of the phase change occurring at the MIT temperature between the VO_2(M1) and the VO_2(R) phases in the temperature range R.T.–350 °C.

3.4. VO_2 films at temperatures in the range 400–550 °C

Increasing the temperature above ~400 °C causes new peaks to appear in the Raman spectrum. The first peak observed, emerges at ~870 cm^{-1} (~450 °C). After the appearance of this peak, three more peaks develop at ~156, 829, and 921 cm^{-1} (curve 6 in Fig. 3a). All these peaks appear mixed with the V_2O_5 phase. Immediately after the appearance of these peaks, the current (resistance) rapidly decreases (increases) with increasing temperature (point 6 in Fig. 3b). Also, above ~400 °C, the current is not stable with time for a given temperature. Fig. 6 shows the time dependency of the current for different temperatures in the range ~325–475 °C. Below 400 °C, the current is reasonably constant with time. Above ~400 °C however, the current starts decreasing with time and the decreasing rate pronounces with increasing temperature. This is especially noticeable at ~475 °C (point 7 in Fig. 3b). At this temperature, the current decreasing rate with time is most pronounced, i.e., from 30 mA down to 50 μA in 60 min (~3 orders of magnitude in current decrease). This pronounced decrease (increase) in current (resistance), coincides with a maximum in the Raman intensity of the new peaks (curve 7 in Fig. 3a). During the current decrease down to 50 μA, the new peaks gradually vanish. At ~ 500 °C, all the peaks in the Raman spectrum can be ascribed to the V_2O_5 phase. Increasing the temperature up to 550 °C does not result in any other change in the Raman spectrum (curve 8 in Fig. 3a). The V_2O_5 phase is observed to remain after the temperature is decreased down to 30 °C (curve 9 in Fig. 3a).

Gilberd et al. [35], studied the thermal oxidation of vanadium in bulk vanadium and He implanted vanadium samples in O_2 at different temperatures. It was observed that in bulk vanadium below 450 °C, oxygen diffused from the growing oxide layer into the bulk following a *log(t)* dependency [35]. In contrast, it was observed that at 450 °C the oxide growth changed to a $t^{1/2}$ dependency. They also observed, a new phase identified as the V_3O_7 phase appearing at 350 and 400 °C. At 350 °C, the V_3O_7 phase was mixed with the VO_2 phase. At 400 °C however, the V_3O_7 phase was the predominant phase (a minor amount of V_2O_5 was also detected). As mentioned in the introduction, V_3O_7 is a valence-mixed oxide phase commonly observed in an oxidation/reduction VO_2–V_2O_5 process. This phase exhibits insulator character at temperatures below 677 °C [7]. These observations suggest that the new peaks appearing in the Raman spectrum above 400 °C (curve 6 in Fig. 3a) may correspond to the formation of the V_3O_7 phase. The insulator character of the V_3O_7 phase would also explain the pronounced current decrease observed in the films at temperatures above ~450 °C (points 6 and 7 in Fig. 3b). Unfortunately, to our knowledge, there is no experimental information about the Raman vibrational modes in pure V_3O_7 crystals and thin films. Thus, in order to confirm this hypothesis, the same protocol detailed in Section 3.3 was performed with a new set of samples, i.e., the temperature was decreased down to 30 °C immediately after the appearance of the new peaks at ~450 °C and N_2 was pumped into the chamber to avoid further oxidation during the cooling process. Fig. 7 shows the Raman spectra at 30 °C. The peaks corresponding to the V_2O_5 phase dominate the spectra and only those most intense peaks of the VO_2 phase at ~195, 223 and 610 cm^{-1} are still observed. This indicates that most of the initial VO_2 of the film has transformed to V_2O_5. The new peaks observed at ~450 °C appear blue-shifted at 30 °C with frequencies at ~167, 845, 881 and 934 cm^{-1}. Also, three peaks not present at ~450 °C were also observed at 30 °C with weak intensities at ~791, 912 and 1033 cm^{-1}. Table 3 summarizes the frequency and FWHM of all these peaks at 30 °C.

The Raman signature for the peaks appearing at ~450 °C has been observed in works with vanadium oxide nanotubes (VONTs) [36,37], and with vanadium oxide thin films deposited by PLD (Pulsed Laser Deposition) from a V_2O_5 target [17]. The crystal structure of the VONT walls has been determined to be very similar to that of ethylene diamine V_7O_{16} [6,38]. In ethylene diamine V_7O_{16}, the amine molecule is embedded between the oxide layers [38]. This prevents the rolling and scrolling of the oxide layers [38]. Recently, the same signature was found in vanadium oxide thin films deposited by PLD [39]. Based on the similarity between the crystals structure of the VONT walls and that of ethylene diamine V_7O_{16}, the observed signature was ascribed to the triclinic V_7O_{16} phase [39]. Unfortunately, V_7O_{16} has never been synthesized as pure bulk crystal and the Raman signature identified. Also, the V_7O_{16} phase has never been detected during the oxi-

dation/reduction process of VO_2–V_2O_5 [13,40]. Thus, in order to confirm the oxidation undergone by the films, XPS measurements were performed for all the oxidation states previously identified.

4. XPS study of the films oxidation states

XPS measurements were performed on eight vanadium oxide films with different oxidation states. Two as-received films, one fabricated on SiO_2/Si and another one on Al_2O_3 were used as a reference for the VO_2 phase. Two more films, one on each type of substrate, were oxidized at 550 °C during 2 h and used as a reference for the V_2O_5 phase. The V_2O_5 phase was confirmed by Raman spectroscopy and no other peaks corresponding to other phases were observed. Finally, one film with similar oxidation state as that observed at 400 °C in Section 3.3 and another with similar oxidation state as that observed at 450 °C in Section 3.4 were fabricated on each type of substrate. These films presented an almost identical Raman signature at 30 °C as those shown in Figs. 4 and 7 and were expected to exhibit a vanadium oxidation state between 4^+ and 5^+, i.e., between that of VO_2 and V_2O_5. Thus, four different degrees of oxidation were analyzed; one for the as-received VO_2 samples (no thermal treatment) and the other three for the samples thermally oxidized at 400, 450 and 550 °C, respectively.

Fig. 8a shows the XPS narrow spectra (O1 s and V2p levels) obtained from an as-received vanadium dioxide film on a SiO_2/Si substrate. The two higher energy peaks relate to the O1 s energy level. The peak at ~530 eV relates to the BE of the O—V bonds. The peak at ~532 eV is ascribable to surface contamination mostly from C bonds (C—O, C=O and C—(OH)). The deconvolution of the $V2p_{3/2}$ and $V2p_{1/2}$ peaks exhibits two components corresponding to the $V4^+$ and $V5^+$ oxidation states, respectively. The presence of the V^{5+} component in the VO_2 samples denotes an over-oxidation, most likely due to the existence of V_2O_5 at the surface of the films from air exposure. The existence of V_2O_5 at the surface has also been reported in vanadium oxides with a high chemical purity [41], and is easily detected by the XPS measurements since the technique is mostly sensitive to the first ~10 nm beneath the surface of the films [42]. Also, the presence of the V_2O_5 at the surface of the films was confirmed by performing a 5-s Ar^+ etching within the XPS chamber. After 5 s of Ar^+ etching, the V^{5+} component in the as-received VO_2 samples was barely discernible (data not shown). Unfortunately, Ar^+ etching is also known to preferentially etch oxygen atoms. This results in a reduction of the oxidation state of the sample which prevents an accurate determination of the oxidation state even if slow ion etching is performed [41].

Figs. 8b–d show the narrow XPS spectrum of the $V2p_{3/2}$ energy levels for the thermally oxidized samples at each oxidation temperature, i.e., 400, 450 and 550 °C. Excellent fittings are obtained in all cases. An average BE for the $V5^+$ component of the $V2p_{3/2}$ signal is found at ~517.3 eV and a FWHM ~1.1 eV. For the $V4^+$ component the average BE is ~516.0 eV and the FWHM ~1.5 eV. These values perfectly agree with those previously reported in the literature [18,19]. Table 4 summarizes all the values for the BE and FWHM of the V2p energy level determined from the XPS experiments.

Several methods have been reported to estimate the oxidation state in transition metal oxides [19]. As already mentioned by Silversmit et al. [19], the classical method based on the sensitivity factors may result in significant inaccuracies when used with transition metal oxides. This is because the sensitivity factors for the 2p binding energies of transition metals largely vary due to the multi-electron processes dependency of the chemical state [43]. Alternatively, an averaged oxidation state can be determined by computing the weighted percentage of the areas (WPA) of the $V2p_{3/2}$ components. In this method, the percentage of each area deconvoluted from the $V2p_{3/2}$ signal is multiplied by an integer factor according to the valence number corresponding to each component. Further details of the WPA technique are given in Ref. [19]. Table 4 details the vanadium oxidation state determined for all the samples by the two methods. In principle, by using the WPA technique and knowing the Ar^+ etching ratio of each oxide stoichiometry it is possible to estimate the fraction or thickness of a given oxidation state. Nevertheless, in order to accurately estimate the thickness of the oxidation layer, accurate values of the etching ratios corresponding to each oxide stoichiometry and correction factors to account for the preferential etching of oxygen atoms are needed at each etching step. This is not done in this work and values in Table 4 refer only to those computed with no Ar^+ etching bombardment. It is also important to mention that compared with the weighted percentage method, the use of sensitivity factors yields systematically smaller values for the oxidation state. This discrepancy between the two methods was also reported in the work of Silversmit et al. [19], and it was concluded that the use of sensitivity factors to determine the oxidation state was not accurate enough. Thus, in this work, only the values from the WPA method will be used.

As shown in Fig. 8, the ratio between the $V5^+$ and $V4^+$ areas in the XPS spectra of the films increases with increasing oxidation temperature. For the films oxidized at 550 °C the estimated vanadium oxidation state is ~4.86. This confirms that these films mainly consist of the V_2O_5 phase. In case of the as-received VO_2 samples, the average vanadium oxidation state is ~4.34. This value is consistent with the over-oxidation observed due to the presence of the $V5^+$ component in the XPS spectrum (Fig. 8a). With respect to the samples heated up to 400 and 450 °C, the estimated vanadium oxidation states are ~4.49 and 4.66, respectively. These oxidation states cannot be ascribed to any specific vanadium oxide phase since the Raman experiments clearly show the existence of a mixture between two or more phases (Figs. 4 and 7). Also, the oxidation state value for the samples heated up to 400 °C coincides with that expected for a balanced mixture of the VO_2 and V_2O_5 phases (as shown by the Raman measurements in Fig. 4). The value is also smaller than that expected in pure V_7O_{16} and V_3O_7, i.e., ~4.57 and 4.66 respectively. This confirms that at this temperature (~400 °C) none of these two phases (V_7O_{16} or V_3O_7) may have been formed in a relevant proportion within the film composition. In contrast, the samples heated up to 450 °C show an oxidation state value identical to that expected in pure V_3O_7 (~4.66) and slightly higher than that of V_7O_{16} (~4.57). Nevertheless, since the films contain V_2O_5 (and some minor amount of VO_2 as identified by the Raman experiments (Fig. 7)), it is possible that the average oxidation state characterized by the XPS technique might be higher than that expected in pure V_7O_{16}. Thus, within the accuracy of the technique it has to be concluded that the oxidation state for the samples heated up to 450 °C is ~4.6–4.7. It is also important to mention that due to the low probing penetration of the XPS technique, the oxidation state values determined in this section are more representative of the surface of the films. Thus, these values are likely to be slightly overestimated compared with those expected for the bulk.

5. Discussion

Based in all the above results, a model to explain the oxidation undergone by the films which account for all the different phenomena observed during the experiments is proposed.

As already mentioned in Section 3.2 in the temperature range ~R.T.–350 °C, upon heating the films above the MIT temperature the initial VO_2(M1) phase changes to VO_2(R). Both phases are clearly identified by Raman spectroscopy. The phase change is reversible with temperature, i.e., a decrease in temperature below the MIT temperature restores the original monoclinic phase. The

Table 4
Vanadium oxidation state, BE and FWHM values determined for the as-received vanadium dioxide films and those oxidized at ~400, 450 and 550 °C. The BE values are charge corrected to the O1 s peak at 530 eV.

	V2p$_{3/2}$ (V^{5+})		V2p$_{3/2}$ (V^{4+})		V2p$_{1/2}$ (V^{5+})		V2p$_{1/2}$ (V^{4+})		Vanadium valence	
Film	BE (eV)	FWHM (eV)	BE (eV)	FWHM (eV)	BE (eV)	FWHM (eV)	BE (eV)	FWHM (eV)	WPA[a]	RSF[b]
VO_2 (as-received)	517.37	1.27	516.10	1.47	524.92	2.40	523.62	2.57	4.34	3.58
VO_x (400 → 30 °C)	517.32	1.24	516.00	1.45	524.64	2.64	523.49	2.72	4.49	4.46
VO_x (450 → 30 °C)	517.23	1.20	515.94	1.50	524.60	2.55	523.42	2.86	4.66	4.40
V_2O_5 (550 2 h → 30 °C)	517.18	0.94	516.03	1.45	524.66	2.60	523.33	2.82	4.86	4.72
Average	517.3	1.1	516.0	1.5	524.7	2.6	523.4	2.8	–	–
Std. Dev.	0.1	0.2	0.1	0.1	0.2	0.1	0.1	0.1	–	–

[a] Calculated from the weighted percentage areas method (WPA).
[b] Calculated from the relative sensitivity factors (RSF).

reversibility of the process is possible due to the negligible oxygen absorption from air in this range of temperatures.

Above ~350–400 °C however, VO_2 progressively transforms to V_2O_5 by absorbing oxygen from the air. The absorption of oxygen in this temperature range is very limited though. The transformation of VO_2 to V_2O_5 originates at the surface and exponentially decreases with increasing V_2O_5 thickness. The poor oxygen absorption in this temperature range limits the amount of VO_2 that transforms to V_2O_5 to a critical thickness. In the Raman spectrum, the V_2O_5 layer growing at the surface is identified by an initial peak appearing at 136 cm^{-1}. This peak is quickly followed by other less intense peaks assigned also to the V_2O_5 Raman signature. At this point, a decrease in temperature down to R.T., do not recover all the initial VO_2, i.e., the VO_2 that has been transformed into V_2O_5 do not revert to VO_2 once the temperature is decreased down to R.T. The amount of transformed V_2O_5 depends on the time that the film has been exposed to air at temperatures above ~350 °C.

Increasing the temperature above ~400 °C accelerates the oxygen absorption from the air and allows the diffusion through the bulk of the film. This allows the VO_2 beneath the V_2O_5 layer at the surface to oxidize. The oxidation rate is however slow compared with that occurring at the surface. The slow oxidation rate and the presence of the top V_2O_5 layer may favor the formation of mixed-valence vanadium oxides with layered structure. This is because layered oxides such as V_6O_{13} and V_3O_7 are constituted by single and double layers of vanadium oxide polyhedra as those of the top V_2O_5 layer [7]. The coexistence and stability of a mixed-valence vanadium oxide phase such as V_6O_{13} and V_2O_5 has already been confirmed by reactive molecular dynamics simulations [44]. In their work, Jeon et al. [44]. studied the surface stoichiometry and chemical stability of several vanadium oxides including VO_2, V_6O_{13} and V_2O_5. After analyzing the charge distribution and the corresponding pair-distribution functions, the authors concluded that VO_2 in proximity to a free surface could evolve into a mixture of V_6O_{13} and V_2O_5. This mixture would be stable in both bulk crystalline and thin films and thus agree with the findings in this work. Also, in the work of Jeon et al. [44], it is suggested that a lower stability of V_6O_{13} compared with that of V_2O_5, may result in V_6O_{13} partially or completely transforming into V_2O_5. The results in this work thus confirm this hypothesis.

During the layered structure formation, water molecules and other particles from the air may diffuse and result trapped between the oxide layers in a similar structure of that of xerogels. The structure of xerogels is known to consist of V_2O_5 bilayers with water intercalated between the bilayers [8,45]. Evidences for the formation of this structure have already been observed within the Raman experiments in this work. First, the peak at ~167 cm^{-1} (at ~30 °C), identified as a layered mode, reveals the formation of a layered structure. Second, the appearance of the peak at ~881 cm^{-1} (at ~30 °C) has already been observed and ascribed to the structure of $V_2O_5{\cdot}nH_2O$ and $V_3O_7{\cdot}nH_2O$ xerogels [45–47]. Finally, two more peaks at ~845 and 934 cm^{-1} (at ~30 °C) have been observed to appear after the occurrence of the 881 cm^{-1} peak. The ~845 cm^{-1} peak has been ascribed to a normally Raman-inactive mode which becomes active in the presence of some structural disorder [16,48,49], and the 934 cm^{-1} mode to the $V4^+ = O$ bonds in amorphous V_2O_5 [33,36]. Thus, the presence of all these modes in the Raman spectrum, fully supports the hypothesis of the formation of a xerogel structure based on a layered oxide. Finally, after the temperature is increased up to 500–550 °C, the Raman peaks observed at ~167, 845, 881 and 934 cm^{-1}, ascribed to the xerogel formation, start vanishing progressively. Thereafter, only those peaks corresponding to the V_2O_5 crystalline phase are observed in the Raman spectrum. It is also important to mention, that despite the differences in thermal conductivity between the SiO_2/Si and the Al_2O_3 substrates, no significant changes in the Raman spectra evolution with temperature were observed for the samples deposited on both substrates from R.T. up to 550 °C (only minor differences in the temperature onset for each phase change were observed with the two substrates). This suggests that the oxidation dynamics and the stability of the top oxidized layer are not significantly compromised depending on the type of substrate. Due to the limitations of the Raman technique however, it is difficult to accurately determine the impact of the substrate on the interfacial layer between the substrate and the vanadium oxide on top.

Despite that the structure of xerogels has been widely studied and several models exist in the literature, the structure and formation of xerogels is not yet completely understood [8,45,50]. Kristoferssen et al. [50] proposed a model for the structure of a $V_2O_5{\cdot}nH_2O$ xerogel to account for the results of existing experiments. In this model, the xerogel structure consists of V_2O_5 bilayers with water intercalated between the bilayers and with the vanadium atoms in the bilayers separated ~2.8–2.9 Å. The xerogel composition has also to conform as a Brønsted acid to explain the presence of H_3O^+ found in previous experiments [8]. Finally, for n values lower than 0.3 the results of previous experiments suggest that the xerogel structure is unstable and assimilates that of crystal V_2O_5 [45,50]. In case of xerogels samples prepared in aqueous medium, the temperature for crystallization occurs at ~350 °C [50]. Above this temperature, the water particles trapped between the oxide layers are desorbed and the structure changes to the orthorhombic V_2O_5 phase. In our work however, the Raman peaks denoting the xerogel formation disappear at ~500 °C. The higher temperature compared with that reported for xerogels prepared in aqueous medium (~350 °C) would be consequence of the heterogeneous composition of the samples used in this work, i.e. Si/SiO_2 or Al_2O_3 substrate, interface and vanadium oxide film and the differences in thermal conductivity between these materials. Thus, from all the above conditions, it is clear that the formation of a xerogel structure is limited within a narrow range of temperatures. In the low temperature limit, the formation of a xerogel is limited by the initial formation of a bilayer structure with water interca-

lated between the bilayers. In the high temperature limit, water is desorbed ant the xerogel structure changes to that of crystal V_2O_5.

Fig. 9 shows SEM images of the vanadium oxide films deposited on SiO_2/Si analyzed in this work at R.T. for different degrees of oxidation. As it can be seen, the morphology of the as-received films (Fig. 9a) and those oxidized at 450 °C and cooled down to 30 °C immediately after the appearance of the Raman peaks at ~156, 829, 870 and 921 cm^{-1} (Fig. 9b) do not show significant differences. However, as observed in Fig. 9c, the morphology of the films oxidized during 2 h at 550 °C drastically changes. This structural change clearly occurs at temperatures above ~450 °C and confirms the hypothesis of an ongoing structural disorder in correspondence with the appearing of the peaks at 845 and 934 cm^{-1}. Also, the vanishing of the Raman peaks when the temperature is increased up to 500–550 °C is consistent with the increase in symmetry from monoclinic V_6O_{13} and V_3O_7, to orthorhombic V_2O_5. From a symmetry point of view, an increase in symmetry involves a reduction in the number of peaks in the Raman spectrum as observed in the measurements.

Thus, from all the above evidences and the observations in Section 3.4, we believe that those structural changes observed in this work at 450 °C, are most likely due to the formation of a xerogel-type structure mediated by an intermediate phase such as that of V_6O_{13} or V_3O_7.

6. Conclusions

The oxidation process of VO_2 thin films deposited on SiO_2/Si and Al_2O_3 substrates with temperature in the range R.T.–550 °C was investigated. The numerous phase changes occurring during the oxidation were monitored by Raman spectroscopy and X-ray photoelectron spectroscopy. Current and resistance measurements on the films were performed in parallel with the Raman measurements to correlate the different phases with the conductivity of the films. Peak frequencies, FHWM, binding energies and oxidation states were reported for all the phases encountered and for the two types of substrates. In addition to the measurements, a model to account for all the phenomena observed during the oxidation process was proposed.

It was found that when the films were heated above the MIT temperature, the phase of the films changed from VO_2(M1) to VO_2(R) and remained in the rutile phase up to 350 °C. Decreasing the temperature down to R.T. completely restored the monoclinic phase. The reversibility of the process at temperatures below 350 °C is possible due to a limited oxygen absorption which prevents the oxidation of the film. When the films were heated above ~350–400 °C however, V_2O_5 was found to be formed at the surface of the films. It was observed that a decrease in temperature down to 30 °C did not restore all the initial VO_2 and the fraction of the film already oxidized did not convert to VO_2. Raman spectroscopy showed that the two phases, VO_2 and V_2O_5, coexisted within the film at R.T. In this temperature range, i.e., ~350–400 °C, there is still little oxygen absorption. This little oxygen absorption, limits the growth of the V_2O_5 layer to a critical thickness. Heating the films above ~400 °C favored the oxygen absorption and allowed oxygen to diffuse towards the bulk of the film. This resulted in the oxidation of the VO_2 beneath the V_2O_5 layer. It was suggested that the presence of the V_2O_5 layer at the surface of the film and the reduced oxygen diffusion favored the formation of a mixed-valence vanadium layered oxide such as V_3O_7. This was supported by the XPS measurements which determined that the vanadium oxidation state at this temperature was ~4.6–4.7. The presence of this mixed-valence vanadium oxide, coincided with a drastic fall in the current of the film which was explained considering the insulator character of the V_3O_7 phase. It was also proposed that a xerogel-type structure may have been formed during the formation of this mixed-valence vanadium layered oxide by absorbing some contaminants from the surface e.g. water particles. These particles would result trapped between the oxide layers and form a xerogel structure. The formation of this xerogel structure was explained from the particular Raman signature observed at this temperature. Finally, this Raman signature was observed to disappear at temperatures above ~500 °C. This was explained by considering that at this temperature the water molecules trapped between the oxide layers might be desorbed and the crystal structure restored to orthorhombic V_2O_5. SEM measurements of the surface of the films confirmed a drastic change in morphology in those films heated above 450 °C.

Acknowledgments

The authors would like to acknowledge Pierre Louette from the Université de Namur and Pierre Eloy from the Université catholique de Louvain for the XPS measurements of the films and the fruitful discussions about the XPS analysis. The authors would also like to thank Annie Beassaudou and Alexandre Boulle from the Université de Limoges for their help with the XRD analysis and the films deposition. This work was supported by the Communauté française de Belgique (Action de Recherches Concertées (ARC)–Stresstronics project) and by the Walloon Region of Belgium (Captindoor project).

References

[1] S. Beke, A review of the growth of V2O5 films from 1885 to 2010, Thin Solid Films 519 (2011) 1761–1771.
[2] M.M. Qazilbash, M. Brehm, B.G. Chae, P.C. Ho, G.O. Andreev, B.J. Kim, S.J. Yun, A.V. Balatsky, M.B. Maple, F. Keilmann, H.T. Kim, D.N. Basov, Mott transition in VO2 revealed by infrared spectroscopy and nano-imaging, Science 318 (2007) 1750–1753.
[3] Y. Ji, Y. Zhang, M. Gao, Z. Yuan, Y. Xia, C. Jin, B. Tao, C. Chen, Q. Jia, Y. Lin, Role of microstructures on the M1-M2 phase transition in epitaxial VO2 thin films, Sci. Rep. 4 (2014) 4854.
[4] A. Pergament, G. Stefanovich, A. Velichko, Oxide electronics and vanadium dioxide perspective: a review, J. Select. Top. Nano Electron. Comput. 1 (2013) 24–43.
[5] C. Julien, G.A. Nazri, O. Bergström, Raman scattering studies of microcrystalline V6O13, Physica Status Solidi (B) 201 (1997) 319–326.
[6] N.A. Chernova, M. Roppolo, A.C. Dillon, M.S. Whittingham, Layered vanadium and molybdenum oxides: batteries and electrochromics, J. Mater. Chem. 19 (2009) 2526.
[7] N. Bahlawane, D. Lenoble, Vanadium oxide compounds: structure, properties, and growth from the gas phase, chem, Vap. Dep. 20 (2014) 299–311.
[8] H.H. Kristoffersen, H. Metiu, Structure of V2O5·nH2O xerogels, J. Phys. Chem. C 120 (2016) 3986–3992.
[9] M.B. Sahana, C. Sudakar, C. Thapa, G. Lawes, V.M. Naik, R.J. Baird, G.W. Auner, R. Naik, K.R. Padmanabhan, Electrochemical properties of V2O5 thin films deposited by spin coating, Mate. Sci. Eng.: B 143 (2007) 42–50.
[10] B.M. Weckhuysen, D.E. Keller, Chemistry, spectroscopy and the role of supported vanadium oxides in heterogeneous catalysis, Catal. Today 78 (2003) 25–46.
[11] K. Waltersson, B. Forslund, K.-A. Wilhelmi, S. Andersson, J. Galy, The crystal structure of V3O7, Acta Cryst. B30 (1974) 2644–2652.
[12] Z. Yang, C. Ko, S. Ramanathan, Oxide electronics utilizing ultrafast metal-Insulator transitions, Annu. Rev. Mater. Res. 41 (2011) 337–367.
[13] Y. Ningyi, L. Jinhua, L. Chenglu, Valence reduction process from sol–gel V2O5 to VO2 thin films, Appl. Surf. Sci. 191 (2002) 176–180.
[14] M. Pan, J. Liu, H. Zhong, S. Wang, Z.-f. Li, X. Chen, W. Lu, Raman study of the phase transition in VO2 thin films, J. Cryst. Growth 268 (2004) 178–183.
[15] P. Schilbe, Raman scattering in VO2, Physica B 316–317 (2002) 600–602.
[16] C. Julien, J.P. Guesdon, A. Gorenstein, A. Khelfa, I. Ivanov, The influence of the substrate material on the growth of V2O5 flash-evaporated films, Appl. Surf. Sci. 90 (1995) 389–391.
[17] V. Théry, A. Boulle, A. Crunteanu, J.C. Orlianges, A. Beaumont, R. Mayet, A. Mennai, F. Cosset, A. Bessaudou, M. Fabert, Role of thermal strain in the metal-insulator and structural phase transition of epitaxial VO2 films, Phys. Rev. B 93 (2016) 184106.
[18] M.C. Biesinger, L.W.M. Lau, A.R. Gerson, R.S.C. Smart, Resolving surface chemical states in XPS analysis of first row transition metals, oxides and hydroxides: sc, Ti, V, Cu and Zn, Appl. Surf. Sci. 257 (2010) 887–898.
[19] G. Silversmit, D. Depla, H. Poelman, G.B. Marin, R. De Gryse, Determination of the V2p XPS binding energies for different vanadium oxidation states (V5+ to VO+), J. Electron. Spectrosc. Relat. Phenom. 135 (2004) 167–175.

[20] C. Marini, E. Arcangeletti, D. Di Castro, L. Baldassare, A. Perucchi, S. Lupi, L. Malavasi, L. Boeri, E. Pomjakushina, K. Conder, P. Postorino, Optical properties of V1-xCrxO2 compounds under high pressure, Phys. Rev. B 77 (2008) 235111.
[21] I.N. Goncharuk, A.V. Ilinskiy, O.E. Kvashenkina, E.B. Shadrin, Electron-electron correlations in Raman spectra of VO2, Phys. Solid State 55 (2013) 164–174.
[22] G.I. Petrov, V.V. Yakovlev, J. Squier, Raman microscopy analysis of phase transformation mechanisms in vanadium dioxide, Appl. Phys. Lett. 81 (2002) 1023.
[23] J.R. Brews, Symmetry considerations and the vanadium dioxide phase transition, Phys. Rev. B 1 (1970) 2557–2568.
[24] A. Zylbersztejn, N.F. Mott, Metal-insulator transition in vanadium dioxide, Phys. Rev. B 11 (1975) 4383–4395.
[25] M. Zaghrioui, J. Sakai, N.H. Azhan, K. Su, K. Okimura, Polarized Raman scattering of large crystalline domains in VO2 films on sapphire, Vib. Spectrosc 80 (2015) 79–85.
[26] F. Ureña, S.H. Olsen, J.-P. Raskin, Raman measurements of uniaxial strain in silicon nanostructures, J. Appl. Phys. 114 (2013) 144507.
[27] R. Lopez, L.A. Boatner, T.E. Haynes, R.F. Haglund, L.C. Feldman, Enhanced hysteresis in the semiconductor-to-metal phase transition of VO[sub 2] precipitates formed in SiO[sub 2] by ion implantation, Appl. Phys. Lett. 79 (2001) 3161.
[28] M.M. Fejer, S. Rowan, G. Cagnoli, D.R.M. Crooks, A. Gretarsson, G.M. Harry, J. Hough, S.D. Penn, P.H. Sneddon, S.P. Vyatchanin, Thermoelastic dissipation in inhomogeneous media: loss measurements and displacement noise in coated test masses for interferometric gravitational wave detectors, Phys. Rev. D 70 (2004) 082003.
[29] R. Srivastava, L.L. Chase, Raman spectrum of semiconducting and metallic VO2, Phys. Rev. Lett. 27 (1971) 727–730.
[30] S. Zhang, I.S. Kim, L.J. Lauhon, Stoichiometry engineering of monoclinic to rutile phase transition in suspended single crystalline vanadium dioxide nanobeams, Nano Lett. 11 (2011) 1443–1447.
[31] R.A. Aliev, V.A. Klimov, Effect of synthesis conditions on the metal-semiconductor phase transition in vanadium dioxide thin films, Phys. Solid State 46 (2004) 532–536.
[32] M. Castriota, E. Cazzanelli, A. Fasanella, D. Teeters, Electrical conductivity and Raman characterization of V2O5 grown by sol–gel technique inside nanoscale pores, Thin Solid Films 553 (2014) 127–131.
[33] S.-H. Lee, H.M. Cheong, M. Je Seong, P. Liu, C.E. Tracy, A. Mascarenhas, J.R. Pitts, S.K. Deb, Microstructure study of amorphous vanadium oxide thin films using raman spectroscopy, J. Appl. Phys. 92 (2002) 1893.
[34] L. Abello, E. Husson, Y. Repelin, G. Lucazeau, Vibrational spectra and valence force field of crystalline V2O5, Spectrochim. Acta A: Mol. Spectr. 39 (1983) 641–651.
[35] P.W. Gilberd, P.B. Johnson, I.C. Vickridge, A.C. Wismayer, TEM and IBA study of the thermal oxidation of V following high dose He implantation, J. Nucl. Mater. 244 (1997) 51–58.
[36] X. Liu, C. Huang, J. Qiu, Y. Wang, The effect of thermal annealing and laser irradiation on the microstructure of vanadium oxide nanotubes, Appl. Surf. Sci. 253 (2006) 2747–2751.
[37] A.G. Souza Filho, O.P. Ferreira, E.J.G. Santos, J. Mendes Filho, O.L. Alves, Raman spectra in vanadate nanotubes revisited, Nano Lett. 4 (2004) 2099–2104.
[38] M. Wörle, F. Krumeich, F. Bieri, H.-J. Muhr, R. Nesper, Flexible V7O16 layers as the common structural element of vanadium oxide nanotubes and a new crystalline vanadate, Z. Anorg. Allg. Chem. 628 (2002) 2778–2784.
[39] J. Huotari, J. Lappalainen, J. Eriksson, R. Bjorklund, E. Heinonen, I. Miinalainen, J. Puustinen, A. Lloyd Spetz, Synthesis of nanostructured solid-state phases of V7O16 and V2O5 compounds for ppb-level detection of ammonia, J. Alloys Compd. 675 (2016) 433–440.
[40] K. Kosugue, The phase diagram and phase transition of the V2O3-V2O5 system, J. Phys. Chem. Solids 28 (1967) 1613–1621.
[41] E. Hryha, E. Rutqvist, L. Nyborg, Stoichiometric vanadium oxides studied by XPS, Surf. Interface Anal. 44 (2012) 1022–1025.
[42] K.A. Wepasnick, B.A. Smith, J.L. Bitter, D.H. Fairbrother, Chemical and structural characterization of carbon nanotube surfaces, Anal. Bioanal. Chem. 396 (2010) 1003–1014.
[43] C.D. Wagner, L.E. Davis, M.V. Zeller, J.A. Taylor, R.H. Raymond, L.H. Gale, Empirical atomic sensitivity factors for quantitative analysis by electron spectroscopy for chemical analysis, Surf. Interface Anal. 3 (1981) 211–225.
[44] B. Jeon, C. Ko, A.C.T. van Duin, S. Ramanathan, Chemical stability and surface stoichiometry of vanadium oxide phases studied by reactive molecular dynamics simulations, Surf. Sci. 606 (2012) 516–522.
[45] L. Abello, E. Husson, Y. Repelin, G. Lucazeau, Structural study of gels of V2O5: vibrational spectra of xerogels, J. Solid State Chem. 56 (1985) 379–389.
[46] I. Mjejri, N. Etteyeb, F. Sediri, Hydrothermal synthesis of mesoporous rod-like nanocrystalline vanadium oxide hydrate V3O7·H2O from hydroquinone and V2O5, Mater. Res. Bull. 48 (2013) 3335–3341.
[47] J. Ma, Q. Wu, Y. Chen, An oxides-hydrothermal approach from bulky V2O5 powder to V3O7·H2O nanoribbons or V3O7 nanoflowers in various ethanol/water mixed solvent, Mater. Res. Bull. 44 (2009) 1142–1147.
[48] A. Gorenstein, The growth and electrochemical properties of V6O13 flash-evaporated films, Solid State Ionics 76 (1995) 133–141.
[49] A.A. Shubin, O.B. Lapina, E. Bosch, J. Spengler, H. Knözinger, Effect of milling of V2O5 on the local environment of vanadium as studied by solid-state 51 V NMR and complementary methods, J. Phys. Chem. B 103 (1999) 3138–3144.
[50] J. Livage, Vanadium pentoxide gels, Chem. Mater. 3 (1991) 578–593.